Wall-slab joint parameter identification of a reinforced concrete structure using possibly corrupted modal data

Hugo Oliveira, François Louf, Estelle Hervé-secourgeon, Fabrice Gatuingt

▶ **To cite this version:**

Hugo Oliveira, François Louf, Estelle Hervé-secourgeon, Fabrice Gatuingt. Wall-slab joint parameter identification of a reinforced concrete structure using possibly corrupted modal data. International Journal for Numerical and Analytical Methods in Geomechanics, 2020, 44 (1), pp.19-39. 10.1002/nag.2994 . hal-02374312

HAL Id: hal-02374312
https://hal.science/hal-02374312

Submitted on 14 Jan 2020

HAL is a multi-disciplinary open access archive for the deposit and dissemination of scientific research documents, whether they are published or not. The documents may come from teaching and research institutions in France or abroad, or from public or private research centers.

L'archive ouverte pluridisciplinaire **HAL**, est destinée au dépôt et à la diffusion de documents scientifiques de niveau recherche, publiés ou non, émanant des établissements d'enseignement et de recherche français ou étrangers, des laboratoires publics ou privés.

Wall-slab joint parameter identification of a reinforced concrete structure using possibly corrupted modal data

H. Oliveira *[1], F. Louf[1], E. Herve-Secourgeon[1,2,3], and F. Gatuingt[1]

[1]LMT, École normale supérieure Paris-Saclay, CNRS, Université Paris-Saclay, 94235 Cachan, France

[2]Électricité de France, R&D Dept., SEISM Institute, F-91120 Palaiseau, France

[3] IMSIA UMR EDF-CNRS-CEA-ENSTA 9219, F-91120 Palaiseau, France

Abstract

In numerical models, the connections among component members are crucial for the prediction of structural behaviour under different type of solicitations. In reinforced structures, the connections are often assumed rigid, what may not be realistic in many practical cases. As alternative, a semi-rigid behaviour depending on a set of independent parameters can be proposed. In this case, a new difficulty arises, which is finding the appropriate values for those parameters. The present study proposes a numerical strategy for identification of the connection parameters based on the Constitutive Relation Error (CRE). To include all available information, an augmented version (Modified CRE) is implemented. The parameters search is iterative and require large amount of system response analysis. To increase the computational efficiency, a reduced order model is adopted. The proposed approach shows low-sensitivity to limited lack of information and also to support condition variability, both of them verified numerically.

*Corresponding author, email: hugoitaime@gmail.com

In this work, experimental tests for a real 1:4 scale structure is utilized for finding the parameters corresponding to the first three modal shapes. A good agreement between numerical predictions and observations is verified, what highlights the accuracy and stability of the proposed numerical approach. The present study may also find applications in the domain of design of experiments.

Keywords— Finite Element Model Updating, Constitutive Relation Error, Semi-rigid joints, Vibrating regime

1 Introduction

In reinforced concrete structures, wall-slab system consists in having walls and slabs concreted monolithically at once, without beams or pillars. The entire *apparatus* of slabs and walls forms a large structural single piece. This system permits high quality control on the building site when compared to other traditional methods (such as beam-column). It also has reduced maintenance costs along the lifespan. It is found in different structural systems including bridges, viaducts, low-rise and tall buildings, nuclear power-plants [1, 2, 3]. The basic structural components are concrete walls and slabs which are widely documented in the literature and in the international codes. In the case of their union, much progress has been achieved for understanding their behaviour along the last decades including the proposition of new assembling methods [4].

Previous works show that connection strength is influenced by the geometrical features of neighbouring elements, and also by loading type and ratios [5]. When low reinforcement ratio is adopted (as for walls and slabs), an overestimation of the shear resistance may be observed at the connection level [6]. The accurate stiffness estimation is crucial, because in this region, a complex combination of stresses is responsible for transmitting the preferred dynamical load path (from slabs to walls until the foundations) [7].

Some experimental studies have been developed for investigating the behaviour of wall-slab connections under earthquake loading. They indicate that increasing the amount of slab reinforcement is not sufficient for strengthen the connection [8, 9]. In terms of topology, it has been observed that anchorage bracing connection has higher strength, higher ductility and less damage as compared to cross-bracing connections for tunnel forms [10]. The connection is also the place for concentration of non-linear phenomena such as crack formation and propagation for both vertical and horizontal

loadings [11].

Considering the entire structure, when different structural elements are joined, numerical investigation point that damage starts at the connection region between slabs and walls [12]. The traditional Finite Element Method (FEM) analysis can be computational time-consuming and some alternatives exist for decreasing computational effort without great accuracy losses. The Framework Method (FWM) may be practicable for wall-slab systems containing openings [13]. Local models of plasticity may be used for representing the damage effects for different seismic load cases [14, 15, 16].

Despite the remarkable progress made in the recent years for structural analysis, additional work is still needed for improving tests and design [17, 18]. Practical applications reveal considerable discrepancies between numerical predictions and experimental results, particularly for dynamic loadings [19]. One alternative for fading these discrepancies is modifying the model input parameters until the correlation of numerical results and test verification satisfies the needed requirements. This process is known in the literature as Finite Element Model Updating, or parameter identification. Several techniques have been proposed particularly concerning the Finite Element Method [20, 21]. Not only local measures can be included, but also the whole field information [22, 23]. Non-deterministic sampling can be used for better identifying global minimum when there is no previous knowledge about the reference parameters [24]. The same principle has found wide applicability in other engineering fields such as soil mechanics and dams where accurate predictions for design parameters have great impact in risk management [25, 26, 27, 28].

Due to its high degree of redundancy, wall-slab connection is often admitted as rigid for practical purposes [29]. In this case, any damage at this region can compromise the global stability because it put at risk the effective load transmission, becoming a weak link. In the present investigation, we propose considering such connection initially as semi-rigid. The idea is similar to those found in elastic joints widely used in the context of framed structures [30]. The advantage is a better control over the effort transmission and accurate predictability under vibrating regimes. However, finding the most representative parameter values is not a simple task because there are no specific tests for this end. So, numerical strategies of parameter identification become imperative in this domain.

One successful technique for model updating is formulating the parameter search as an optimization problem using the concept of Constitutive Relation Error (CRE) [31, 32]. This concept

was originally developed for measuring the quality of approximate solutions, and since then, the CRE has been developed and validated in distinct application areas including the complex phenomena of damping [33]. Based on a strong physical sense, the CRE has been demonstrated to be a robust performance measure [34].

In the present study, the connection between structural elements are assumed semi-rigid. Then we propose a numerical procedure based on the CRE formulation for identifying the corresponding set of elastic parameters. The procedure is designed to consider all information available from the vibrating regime. The algorithm robustness is manifested on its ability to handle support condition variabilities and also a limited lack of information. As application, the model predictions are compared to experimental results to assess its practical usability and stability.

2 CRE Problem formulation

2.1 Continuous form

Let Ω represent the domain of interest for the present study. The solid is composed of independent deformable solids, $\Omega_i \subset \mathbb{R}^3$, each with boundary, $\partial\Omega_i$. The environmental actions can be specified by displacement constraints $\mathbf{U}_{d_i}$ on a part $\partial_1\Omega_i \subset \partial\Omega_i$, and traction forces $\mathbf{F}_{d_i}$ on $\partial_2\Omega_i \subset \partial\Omega_i$, for any instant of time $t \in [0, T]$. The constraints are applied on complementary parts of each body, $\partial_1\Omega_i \cup \partial_2\Omega_i \cup \Gamma_{ij} = \partial\Omega_i$. The connection region among two arbitrary domains is noted $\Gamma_{ij} = \partial\Omega_i \cap \partial\Omega_j$. The body forces are denoted $\mathbf{f}_{d_i}$ acting through the domain Ω_i. A schematic structure composed of two plates is shown in Figure 1.

The core aspect of CRE theory is separating the governing equations in the following two distinct categories [32]: the *reliable* field comprises all equations that must be strictly respected, and the *unreliable* field include only the equations susceptible to be doubtful. The choice of which equation belongs to which category is not unique. It is the designer who is responsible for evaluating the best scenario according to the problem to be solved. In the present case, the following categories are adopted.

Category 1: The field is reliable whenever it holds:

- Kinematic admissibility. The displacement field is kinematically admissible, $\mathbf{U}_i \in \mathscr{U}^i$, whenever it satisfies:

- Regularity conditions,
- Initial conditions, $\forall M \in \Omega_i$

$$\mathbf{U}_i(t=0) = \mathbf{U}_i^0, \quad \frac{d\mathbf{U}_i}{dt}(t=0) = \dot{\mathbf{U}}_i^0 \tag{1}$$

- Constraints conditions: $\forall t \in [0,T]$,

$$\mathbf{U}_i|_{\partial_1\Omega_i} = \mathbf{U}_{d_i} \tag{2}$$

- Substructure/interface compatibility: $\forall t \in [0,T]$,

$$\mathbf{U}_i|_{\Gamma_{ij}} = \hat{\mathbf{U}}_i \tag{3}$$

It is defined the homogeneous constraint displacement field in $\Omega_i \times [0,T]$:

$$\mathscr{U}_0^i = \{\mathbf{U}_i(M,t) \in \mathscr{U}^i, \mathbf{U}_i(M,t)|_{\partial_1\Omega_i} = 0\}$$

- Dynamic admissibility. The stress field is dynamically admissible, $\sigma_i \in \mathscr{S}^i$, if $\forall t \in [0,T]$, $\forall \mathbf{U}_i^* \in \mathscr{U}_0^i$, then it holds:

$$\int_{\Omega_i} \left(\rho_i \frac{d^2\mathbf{U}_i}{dt^2} + \mathbf{f}_{d_i}\right) \cdot \mathbf{U}_i^* d\Omega_i + \int_{\Omega_i} Tr(\sigma_i \varepsilon(\mathbf{U}_i^*)) d\Omega_i = \int_{\partial_2\Omega_i} \mathbf{F}_{d_i} \cdot \mathbf{U}_i^* d\partial\Omega_i + \int_{\Gamma_{ij}} \sigma_i n \mathbf{U}_i^* d\Gamma \tag{4}$$

- Substructure/interface compatibility: $\forall t \in [0,T]$

$$\sigma_i n|_{\Gamma_{ij}} + \hat{\sigma}_i n|_{\Gamma_{ij}} = 0 \tag{5}$$

- Substructure Constitutive relation field.
  - Material behaviour. The constitutive material of each independent solid is assumed homogeneous, isotropic and linear. The material model is expressed by:

$$\forall M \in \Omega_i, \forall t \in [0,T] \quad \sigma_i = K_i \varepsilon(\mathbf{U}_i) \tag{6}$$

where K_i is the material Hooke tensor and $\varepsilon(\mathbf{U}_i)$ is the small strain tensor.

Category 2: The field is unreliable for the following expression:

$$\hat{\mathbf{R}}|_{\Gamma_{ij}} = C(\hat{\mathbf{U}}_i - \hat{\mathbf{U}}_j) \quad \forall M \in \Gamma_{ij}, \forall t \in [0,T] \tag{7}$$

These categories are valid for each entity separately. The hat in expressions (3) and (5) indicates the interface quantities. To solve the mechanical problem, it is necessary to specify how the hatted quantities are related. It is worth mentioning the formulation enables exploring different constitutive relations for representing various interface behaviours. In the present study, the connections are assumed having no mass and linear response, which is expressed by the relation (7). C stands for Hooke operator depending on a set of real parameters, $\boldsymbol{\theta}$.

According to the CRE theory, it is important to define a functional for measuring the quality of a given solution. Let the pair $(\mathbf{U}, \sigma) = s$ be admissible, i.e. it verifies the reliable equations. For a given solution s, the functional E^2_{RdC} has the following properties:

$$E^2_{RdC}(\mathbf{U}, \sigma) \geqslant 0 \tag{8}$$

$$E^2_{RdC}(\mathbf{U}, \sigma) = 0 \Leftrightarrow (\mathbf{U}, \sigma) \text{ satisfies exactly the unreliable equations} \tag{9}$$

In the present study, the performance functional is specified along the interface region, but not exclusively. It may also include the support conditions because they can be interpreted as interfaces between the structure and the ground. This measure is expressed by the following equation:

$$E^2_{RdC} = \frac{1}{2}\int_{\Gamma_{ij}} (\hat{\mathbf{R}}|_{\Gamma_{ij}} - C(\hat{\mathbf{U}}_i - \hat{\mathbf{U}}_j)) C^{-1} (\hat{\mathbf{R}}|_{\Gamma_{ij}} - C(\hat{\mathbf{U}}_i - \hat{\mathbf{U}}_j)) d\Gamma_{ij} \tag{10}$$

The intended applications consist of structures under vibrating regime. In this case, the inverse problem needs to include all information collected from the data acquisition system. In general, this information can be transformed into displacements for modal analysis. To consider these displacement measures, the performance functional needs to be augmented [35]. The new functional is called Modified Constitutive Relation Error (MCRE) and it is defined as follows:

$$\begin{aligned} \eta^2 = \frac{1}{2}\int_{\Gamma_{ij}} (\hat{\mathbf{R}}|_{\Gamma_{ij}} - C(\hat{\mathbf{U}}_i - \hat{\mathbf{U}}_j)) C^{-1} (\hat{\mathbf{R}}|_{\Gamma_{ij}} - C(\hat{\mathbf{U}}_i - \hat{\mathbf{U}}_j)) d\Gamma_{ij} \\ + \frac{1}{2}\frac{r}{1-r} (\Pi\mathbf{U} - \tilde{\mathbf{U}}(\omega)) G_u (\Pi\mathbf{U} - \tilde{\mathbf{U}}(\omega)) \end{aligned} \tag{11}$$

Note that equation (10) and (11) are quadratic forms. Both the functionals are in agreement

with the properties expressed in equations (8) and (9). In expression (11), G_u is defined as the Hookean operator condensed at the points where the displacement field is being measured. $\tilde{\mathbf{U}}(\omega)$ stands for the measured field at a specific frequency. r is a real number belonging to interval $[0, 1)$ that permits agreeing more confidence to the model or to the reference measures. The field $\hat{\mathbf{U}}_i$ is a subset of $\mathbf{U}_i$. The effort transmission at the interface is controlled by the set of real parameters, $C = C(\boldsymbol{\theta})$. Any changes in $\boldsymbol{\theta}$ have an implicit influence on $\mathbf{U}_i$, and consequently, on $\hat{\mathbf{U}}_i$. In this case, η^2 is a function of $\boldsymbol{\theta}$ and the searched joint parameters correspond to those minimizing the quantity expressed by equation (11).

The final problem can be written in a continuous form as follows:

Problem 1

Find the parameter set $\boldsymbol{\theta}$ such that:

- each pair $(\sigma_m, \mathbf{U}_m)$ belongs to the admissible set of reliable equations;
- $\boldsymbol{\theta}^*$ minimizes $\eta^2(\boldsymbol{\theta})$ (equation (11)).

It is worth mentioning σ depends on dynamical admissibility conditions, whereas $\mathbf{U}$ is originated from the compatible kinematically admissible field. When both of them respect the connection constitutive relation (equation (7)), mathematically, the value of E^2_{RdC} becomes zero. However, for real-world application this norm rarely comes to zero due to several sources of uncertainties, for example, measurement noise, presence of neglected non-linear phenomena, further modelling errors, etc. In despite of that, the solution depends continuously on C which represents the key aspect for the identification procedure.

2.2 Discrete form

The *Problem 1* is solved using the standard FEM formalism. Let $\{U\}$ be the discrete kinematically admissible field, $\{V\}$ is the corresponding dynamical admissible field, $\{\tilde{U}\}$ is the discrete field measures, $[C(\theta)]$ is the connection constitutive matrix, and $[\Pi]$ and $[\Xi]$ are projector matrices. The discrete version of MCRE is written as follows:

$$\eta^2(U, V, \theta) = \frac{1}{2}\{[\Pi](U - V)\}^T [C(\{\theta\})] \{[\Pi](U - V)\} + \frac{1}{2}\frac{r}{1 - r}\{[\Xi]U - \tilde{U}\}^T[G_u]\{[\Xi]U - \tilde{U}\} \quad (12)$$

The dynamical equilibrium equation is included using the Lagrangian augmented form expressed

by:

$$L(U,V,\theta,\lambda) = \frac{1}{2}\{[\Pi](U-V)\}^T\left[C(\{\theta\})\right]\{[\Pi](U-V)\} + \frac{1}{2}\frac{r}{1-r}\{[\Xi]U-\tilde{U}\}^T[G_u]\{[\Xi]U-\tilde{U}\} - \{\lambda\}^T\left([K]\{V\} - \omega^2[M]\{U\} - \{F\}\right) \quad (13)$$

The pair of admissible fields is obtained from the stationarity of the augmented Lagrangian maintaining $\{\theta\}$ fixed at a given ω. Let $\{\theta\}^f$ represent the fixed parameter set, and $[C(\{\theta\}^f)] = [C]$. The stationarity condition is expressed when:

$$\frac{\partial L}{\partial U} = [\Pi]^T[C][\Pi]\{U-V\} + \frac{r}{1-r}\left[G_u\right]\{[\Xi]U-\tilde{U}\} + \omega^2[M]\{\lambda\} = \{0\} \quad (14)$$

$$\frac{\partial L}{\partial V} = [\Pi]^T[C][\Pi]\{U-V\} + [K]\{\lambda\} = \{0\} \quad (15)$$

$$\frac{\partial L}{\partial \lambda} = [K]\{V\} - \omega^2[M]\{U\} - \{F\} = \{0\} \quad (16)$$

These equations can be written in a linear system form:

$$\begin{bmatrix} [\Pi]^T[C][\Pi] & \frac{r}{1-r}[G_u] & \omega^2[M] \\ [\Pi]^T[C][\Pi] & 0 & [K] \\ -[K] & [K]-\omega^2[M] & 0 \end{bmatrix} \begin{Bmatrix} U-V \\ U \\ \lambda \end{Bmatrix} = \begin{Bmatrix} \frac{r}{1-r}[G_u][\Xi]\tilde{U} \\ 0 \\ F \end{Bmatrix} \quad (17)$$

The matrix $[C]$ and $[K]$ depend on the vector parameter $\{\theta\}^f$, so does the solution of the linear system. Using the output quantities $\{U\}$, $\{V\}$ and $\{\lambda\}$ from equation (17), the norm expressed by equation (12) provides a direct way to calculate the sensitivity with respect to $\{\theta\}$ at the fixed set $\{\theta\}^f$. This dependence can be found using the Lagrangian for a given ω:

$$\frac{\partial}{\partial\theta_i}\eta^2(\theta) = \frac{\partial}{\partial\theta_i}L(U(\theta),V(\theta),\lambda(\theta),\theta) \quad (18)$$

$$\frac{\partial}{\partial\theta_i}\eta^2(\theta) = \underbrace{\frac{\partial L}{\partial U}}_{=0}\frac{\partial U}{\partial\theta_i} + \underbrace{\frac{\partial L}{\partial V}}_{=0}\frac{\partial V}{\partial\theta_i} + \underbrace{\frac{\partial L}{\partial \lambda}}_{=0}\frac{\partial \lambda}{\partial\theta_i} + \frac{\partial L}{\partial\theta_i} \quad (19)$$

The quantities $\frac{\partial L}{\partial U}$, $\frac{\partial L}{\partial V}$ and $\frac{\partial L}{\partial \lambda}$ are null because they come from the Lagrangian stationariness. It comes:

$$\frac{\partial}{\partial\theta_i}\eta^2(\theta) = \frac{\partial L}{\partial\theta_i} \quad (20)$$

$$\frac{\partial}{\partial\theta_i}\eta^2(\theta) = \frac{\partial}{\partial\theta_i}\left[\frac{1}{2}\{[\Pi](U-V)\}^T\left[C(\{\theta\})\right]\{[\Pi](U-V)\} + \frac{1}{2}\frac{r}{1-r}\{[\Xi]U-\tilde{U}\}^T[G_u]\{[\Xi]U-\tilde{U}\} - \{\lambda\}^T\left([K]\{V\} - \omega^2[M]\{U\} - \{F\}\right)\right] \quad (21)$$

It leads to the final expression for the gradient of the Modified Constitutive Relation Error (12):

$$\nabla_i = \frac{\partial}{\partial\theta_i}\eta^2(\theta) = \frac{1}{2}\{U-V\}^T[\Pi]^T\frac{\partial[C(\{\theta\})]}{\partial\theta_i}[\Pi]\{U-V\} - \{\lambda\}^T\frac{\partial[K]}{\partial\theta_i}\{V\} \quad (22)$$

The classical steepest gradient approach was utilized for updating the design variables. However, other algorithms may perform better such as Newton or BFGS. Despite the fact that the system from equation (17) is linear, it may become computationally expensive for real-world structures. In this case, Model Order Reduction (MOR) is an available technique for improving efficiency. Let the reduced quantities be identified by subscript R and be written as follows:

$$\{X\} = [H]\{X_R\}\ , \quad \forall\ \{X\} \text{ equal to } \{U\}\ ,\{V\}\ ,\{\lambda\}\ , \quad (23)$$

$$[K_R] = [H]^T[K][H]\ ,\ [M_R] = [H]^T[M][H]\ ,\ [G_{uR}] = [H]^T[G_u][H]\ ,\ [C_R] = [H]^T[C][H], \quad (24)$$

in which $[H]$ denotes reduced basis. The reduced basis consists in a truncated real modal basis which is built by taking N real eigenmodes $\{\phi_i\}$, $i = 1$ to N [36]. Substituting equations (23) and (24) into linear system given by equations (17) yields to a much smaller linear system to solve whose dimension is three times those reduced basis:

$$[A_R]\{X_R\} = \{B_R\}, \quad (25)$$

where $[A_R]$, $\{X_R\}$ and $\{B_R\}$ are expressed as follows:

$$[A_R] = \begin{bmatrix} [\Pi_R]^T[C_R][\Pi_R] & \frac{r}{1-r}[G_{uR}] & \omega^2[M_R] \\ [\Pi_R]^T[C_R][\Pi_R] & 0 & [K_R] \\ -[K_R] & [K_R]-\omega^2[M_R] & 0 \end{bmatrix}\ , \quad (26)$$

with

$$\{X_R\} = \begin{Bmatrix} U_R - V_R \\ U_R \\ \lambda_R \end{Bmatrix} \quad \text{and} \quad \{B_R\} = \begin{Bmatrix} \frac{r}{1-r}[G_{uR}][\Xi]\tilde{U} \\ 0 \\ F_R \end{Bmatrix}. \tag{27}$$

These equations can be implemented using the majority of FEM purpose software. In the present study, Cast3m software [37] was used for implementing the procedure described in Algorithm 1.

Algorithm 1 Proposed task sequence

procedure SetInputData
    Load geometry, material, mesh, fixing conditions
    Set the initial parameter set $\{\theta\}$
procedure SetReferenceMeasure
    Load the available experimental measures
loop:
Obtain the pair of dynamical and kinematical admissible fields (Equation (25))
Calculate the MCRE (Equation (12))
if *MCRE* > *Tolerance* **then**
    Calculate the gradient ∇_i from Equation (22).
    $\theta_i \leftarrow \theta_i + \alpha\nabla_i$.
    goto *loop*
else
    goto *endloop*
endloop:
procedure PostProcessing
    Post treat all required information

3 Application to a representative reinforced concrete structure

3.1 Presentation of the structure

In the present section, we describe how the MCRE norm can be helpful on real world situations. The structure under interest is a 1:4 reduced scale model of a representative reinforced concrete wall-slab junction, with usual construction provisions in nuclear industry. This reinforced concrete structure (herein referred to as mock-up) is used for validating purposes of numerical models con-

sidering dynamical actions. The experimental tests were performed at CEA (French Alternative Energies and Atomic Energy Commission), by means of the AZALEE shaking table, as part of research program launched and funded by Electricité De France (EDF) and CEA [38]. The mock-up geometrical perspective is showed in Figure 2. The material parameters adopted in the following exposition are shown in Table 1 and the geometrical dimensions are illustrated in Figure 3.

The physical mock-up is represented by a numerical model (Figure 4) developed with Cast3m [37]. The supporting mesh is composed by 616 quadrilateral shell elements and 60 three-dimensional beam elements. The gap between the bottom wall and the shaking table is handled by kinematic relations. The physical joints are classified into 4 types, as shown in Figure 4. Connection type 1 represents the four top pillar joints. Connection type 2 encompasses the four bottom pillar joints. Connection 3 represents the two joints below the wall. Connection wall-slab represents the physical union between both structural members. Each connection can have at most 6 linear stiffness (three translational and three rotational) according to each Cartesian axis. These stiffnesses control the transmission of efforts, and the total number of parameters to be identified can reach up to 24. It is not evident such identification because it depends on the amount and quality of the available information and also in the interrelation among the parameters. These aspects are further discussed hereafter.

The experimental mock-up possesses accelerometers distributed along all structural members. The measures are made for translation according to the three axes. The corresponding position on the numerical model is illustrated by small points in Figure 5. Note that there are sensors near the fixation region in order to capture eventual movements in these regions. There are also sensors located on the vibrating table which are used to verify the eventual differential deformation referring to the mock-up connection supports.

3.2 The effects of corrupted data

Essentially every measure of any physical system is uncertain. Part of this uncertainty is statistically intrinsic and depends on the available measurement devices. It is distinct from the systematic error, where other manageable sources of variabilities are present. The idea behind this application is showing how the MCRE can be helpful in finding corrupted data. To achieve this, the numerical model showed in Figure 4 is used to create controlled corrupted modal measures. The target parameter is the rotational stiffness around y, under the wall (Connection 3). Its reference

value is $1.76 \times 10^7 N.m/rad$. The corrupted data is generated by choosing one sensor randomly and inverting its measurement axis. Note that, when fixing the sensors in the experimental apparatus, it is not rare to reverse the measuring axes especially when there are numerous sensors to be installed.

The effects of the corrupted data are shown in Figure 6. The integrate reference data makes the MCRE norm tend to zero before convergence. This behaviour is not the case when the corrupted data is utilized. The reason is that the shape predicted by the defective sensor cannot be met by the numerical model under hypothesis of continuity. This gap between model and measure creates a residue in the second term of equation (12) that can be minimized, but not brought to zero. This residue is observed on the flat part of the graphic. In terms of parameter convergence (Figure 7), it is possible to see that both reference data lead to the same value for the identified parameter. The corrupted data slows the convergence process due to the loss of gradient predictability in localized regions. However, the algorithm maintains its robustness and stability in finding the correct parameter. The next question is: in what extent?

To identify the limits of procedure robustness, the number of defective sensors is increased and the effects are monitored by the change on the behaviour of the MCRE norm. Let CS stands for Corrupted Sensor. The evolution of MCRE according to the number of CS is shown in Figure 8. The number of CS varies from 0 to 15 (around 40% corrupted data). It can be seen the negative effect for the identification process. The MCRE norm loses its quadratic-like behaviour and eventually become flat or monotonically increasing. In this situation, the target parameter cannot be correctly identified.

It is important to verify whether the mesh refinement has impacted these results or not. For this purpose, three meshes containing increasing number of finite elements are defined such as: Level 1 contains 616 elements, Level 2 contains 2344 elements and Level 3 contains 5224 elements. The three meshes are illustrated in Figure 9. Then, the numerical test for identifying rotational stiffness is performed for each mesh assuming no corrupted sensors. The results can be seen in Figure 10. The refinement level seems to impact the cost function history, in particular, far from the convergence point. However, the identified parameter remains the same in all cases. This suggests that good estimations of searched parameter can be obtained even in the presence of relatively coarse meshes. In real world problems, complex meshes are often the case, what makes successive refinements impractical. In these cases, stability, in terms of mesh dependence, is extremely valuable. Based on these results, the Level 1 mesh is assumed in all analysis hereafter.

For sake of efficiency, not all connections need to be updated at the same step in the numerical procedure. The MCRE is helpful in deciding whether a joint should be updated or not. This choice is guided by the contribution that each connection gives to the global MCRE measure. For that, the first term of equation (12) serves as corrector indicator. The more the joint contributes to the MCRE, the greater is the indicator and the more its parameters are updated. The corrupt data can also impact this process.

In Figure 11, it is shown the evolution of the corrector indicator for each connection from 1 to 4 (4 represent the wall-slab connection) for the initial step without loss of generality. The increase of the number of corrupted sensors are represented along the depth direction. According to this figure, when there is no data corruption, the numerical procedure should update the connection 1. This choice is unchanged up to reach 8 CS with a certain robustness. However, when there are 15 CS, the indicator will point out the connection 2 should be updated instead of 1. The decision on which parameters to update can be misguided due to data corruption.

The norm presented in equation (12) still provides further information concerning corrupt data. The second term is related exclusively to the reference measures. Let τ_i represent the partial contribution of the i-th sensor. The operator $[G_u]$ can be diagonal and located only at the specific location of each sensor. In this case the norm results a scalar value representing the local deviation from the reference shape. Let ns be the number of data sensors, one can define the following expression:

$$\tau_i = \frac{\{[\Xi]U - \tilde{U}\}^T [G_u]_i \{[\Xi]U - \tilde{U}\}}{\sum_{l=1}^{ns} \{[\Xi]U - \tilde{U}\}^T [G_u]_l \{[\Xi]U - \tilde{U}\}} \tag{28}$$

Considering the 38 sensors available, it is illustrated in Figure 12 the overall contribution when there is no data corruption. Note that there are no appealing values among them. Even contributions around 17% appears 4 times for the sensors 35, 36, 37 and 38. This value is about three times superior when compared to the second highest (6%), but still not exclusive. Note the difference in Figure 13 where one corrupt sensor is present. The sensor number 10 responds alone for 60% of global error measure which is at least six times superior than the second highest value. This is exactly the sensor used for generating the data corruption. The same behaviour is observed when an additional sensor is considered corrupted. As shown in Figure 14, sensor 10 and 27 responds for about 40% and 33% respectively of the global error measure. These values are at least six times greater than the second highest.

Considering this information as indicator of data corruption, it is possible to focus attention into these specific sensors. In this case, the source of data errors can be investigated and the designer can decide whether the information can be still used or not. Suppose both sensors are suppressed from the analysis. The new error measure contribution among the remaining sensors is showed in Figure 15. Note the resemblance to the case having no data corruption (Figure 12), now with two sensors less than previously.

Systematic errors can corrupt the information and have a negative impact on the parameter identification process. The proposed MCRE formulation manifest a certain robustness to them but is not immune, as any numerical approach. The major feature that can be retained from this application is the fact that the proposed norm in equation (12) is a multivalent quantity. In addition to serve as cost function and gradient calculation, it can be used for investigating the eventual existence of corrupted data in the available information, and even serve to localize it. In an identification algorithm, the model term may indicate which areas should be updated instead of updating all areas at the same time. In other terms, it can behave as a filter. It is evident that the control of input data is a crucial point. Provided the noise stays under accepted limits, the proposed procedure can identify the intended parameter accurately.

It is worth mentioning that systematic errors might be better treated using different norm propositions, in particular, less sensitive to input data errors. This is not a simple task from a deterministic point of view. In this case, probabilistic approaches can be helpful in dealing with different sources of errors at the same time [39]. Despite being promising, probabilistic cost functions were not investigated in the present study.

3.3 The effects of boundary condition perturbations

Understanding the influence of boundary conditions is another key factor for both static and dynamic actions. In statics, depending on the support positions it is possible to obtain structures less compliant [40]. In dynamics, the existing supports can directly affect the low-frequency vibration regime of a structure. The inspiration for that comes from the experiments. It is remarked that ideal boundary conditions are rarely met in complex structural experiments. For example, fixed support conditions are essentially unachievable because all materials manifest deformation, even very small ones. A more realistic condition is semi-rigid supports as those simulated in the present application. So, the question is: if the real boundary conditions do not behave as ideally

assumed, is the process of identification influenced? If so, in which manner?

To address these questions, we propose a methodology using a controlled perturbation of the boundary conditions. The reference structure has ideal pinned condition at connection 1, perfect transmission of efforts at wall-slab joint, semi-rigid supports at connection 2 (Reference value $k_y = 1 \times 10^7 N \cdot m$) and 3 (Reference value $k_{\theta_y} = 1.76 \times 10^7 N \cdot m/rad$). Then we decrease 15% in the stiffness at a given connection along a given direction to allow relative displacements. The decrease occurs at connections other that where the target parameter is located. The idea is checking if the target parameter inside a specified connection can still be identified when the other connections around are perturbed.

The graphic shown in Figure 16 illustrates the response captured by the MCRE norm for identifying the rotational rigidity at connection 3. Three cases are shown. The first one is when there is no perturbation at any connection. The second is named Independent Perturbation (IP). It occurs when the parameter being perturbed does not affect the parameter being identified. In this example, the perturbed parameter is the translational stiffness along the y direction at connection 2. Although the MCRE norm does not assume the same values along the range, it presents the same minimal point. So essentially, this kind of fluctuation is not problematic. The third class of perturbation is called Dependent Perturbation (DP). It occurs when the perturbed parameter disturbs the target parameter identification. In this case, there is some unknown relation between the two variables that affects directly the cost function. The perturbed parameter now is the translational stiffness along the z direction at connection 2. When it occurs, the target parameter is still identified but it is underestimated. Note how this fluctuation can mislead the convergence process.

A similar behaviour is observed for the second target parameter (translational rigidity along y direction at connection 2). In Figure 17, it is shown the identification comparison. The IP perturbing parameter is the rotational rigidity along the x direction at connection 1. The DP parameter is the translational stiffness in along the z direction at the same connection. The IP perturbation keeps almost unchanged the MCRE values whereas the DP overestimates the searched parameter value. This effect can be problematic because the gradient optimization method can easily fall into local minimum induced by the unknown interrelation among the support conditions.

The graphs plotted in Figures 16 and 17 were obtained using the first three modes of vibration. The choice of which mode should be used for identifying a given parameter can also be challenging.

The target parameter now is the translational rigidity along z direction at the wall-slab junction (Reference value $k_z = 1 \times 10^7 N \cdot m$). The DP parameter is the rotational rigidity along y direction at connection 2, whereas the IP parameter is the translational stiffness along x direction at connection 1. It is shown in Figure 18 the evolution of the MCRE norm considering only the mode 1 or mode 2. None of them are able to identify correctly the parameter searched even in the absence of perturbation. However, when the third mode shape is considered, the parameter can be identified as shown in Figure 19. The same pattern previously observed appears with overestimation of the target parameter for DP. The key reason for understanding this effect is the modal shape. In order to identify a certain parameter, in general, one should dispose of a modal shape that mobilizes enough energy where the identification is expected. Otherwise, the updating procedure risks being unable to identify the wanted parameter.

To conclude, the answer for the question posed is positive under certain conditions. The perturbation on the boundary conditions can still permit the identification of parameters at the distinct connections. When the perturbations can be classified as IP, it poses no problem. However, when the estimated perturbations are DP type it can disturb the convergence procedure and misguide the algorithm. In this case, further care must be taken in order to mitigate these effects. It is worth mentioning the possibility of enlarging the set of available information. Actions such as increasing the amount of measure points or the number of measured modal shapes may lead a DP to become an IP type.

3.4 Identifying the assembling rigidity

In the real world, all the above-mentioned effects occur simultaneously and a clear distinction of their causes is rarely possible. In such a case, the previous discussions become handful for eliminating spurious error sources that disturb the identification process. As a final application, the intention now is finding the suitable parameters set that best represents the first three mode shapes and frequencies observed on the experimental mock-up.

When dealing with identification problem under dynamic regime, it is important to have proper estimates for effective masses. Comparing both models in terms of total mass, the experimental estimation is 5.780 kg whereas the numerical mock-up is 5.776 kg. The good correspondence between these two values shows the suitable mass parameters assumed for the remaining steps.

An important aspect is choosing which parameters need to be updated. There is no fixed rule

for that. As a sign, the mock-up metallic supports manifest certain flexibility when the experiment is performed. The slight movement observed correspond ideally to the rotation around the y axis and translation along the z axis, both at connection 3. Based on such observations we chose to update solely these two parameters. The remaining directions of effort transmission are assumed ideal.

In Figure 20, it is shown the MCRE as function of the rotational rigidity for the first mode of vibration. The point of minimum value is $1.71 \times 10^7 N \cdot m/rad$ and it corresponds to the searched parameter. For the second parameter, the remaining two modes are used. Note that the second mode does not permit its identification (Figure 21). Constant values of MCRE indicate that the evolution of the parameter under question does not affect the cost function, or it is irrelevant to the model. However, it happens for a specific mode. When the third mode is utilized, it becomes possible to identify it. The value for the translational rigidity along z axis is $1.94 \times 10^8 N/m$.

The addition of these parameters to the initial model results in the model updated. The new modes and frequencies updated are shown in Figure 22, Figure 23 and Figure 24. Essentially, no substantial changes are observed on the modal shapes; that is a good feature because the initial model possesses modal shapes close to the observed experimentally. So, the identification process did not imply in shape losses. The crucial improvement occurs in terms of frequencies. The numerical frequencies reach a good agreement with the real mock-up.

These results were obtained considering the selection and exclusion of the information from six sensors. In order to show the impact that this choice represents, we repeat the calculations considering all the information available. The results are resumed in Table 2 and Table 3. Three study cases are compared. The first one is the comparison with the initial numerical model considering support conditions ideally pinned. The second case is obtained making the updating based on all sensors available. The final case shows the identification carried out after selection and removing the information from six sensors based on the methodology described on the item 3.2. It is observed an improvement in the prediction capacity of the first three modal frequencies. The same trend is observed in the Modal Assurance Criterion (MAC) showed in Figure 25.

These results permit to infer that the boundary conditions should effectively not be considered as ideally pinned. The identified parameters show that a semi-rigid behaviour is an approach closer to reality.

As can be seen, both the parameters identified represent a good choice for the problem posed.

When the identified parameters do not correspond to the expected frequencies or shape, a possible alternative is reviewing the hypothesis made on the assumed ideal connections. It may be necessary to include other directions of effort transmission to be updated and performing the calculation again. Often this task can be automated.

4 Conclusion

The present study concerned the numerical identification process. It was employed an algorithm based on the Modified Constitutive Relation Error considering the joint parameters as source of doubt. The approach enables the free choice on which parameter the designer wants to update. The algorithm is basically an optimization problem which requires many calls of the numerical model. To improve the computational efficiency, two main features were implemented: the model reduction technique and the analytic gradient calculation.

The numerical investigation is focused on a real-world structure. The results show the capabilities of the MCRE in terms of improving the parameter identification task so important in the engineering context. The norm MCRE serves to several purposes such as being cost function and calculating the sensibilities. In addition, it contains information about parameters having priority to be updated which is a valuable information for complex problems. Also, the norm contains information about possible defective sensors and it can actually serve as filter of information. All these features together make it a robust quantity beneficial to the domain of Inverse Problems for parameter investigation.

As perspective, more complex support conditions can be proposed including friction and viscous responses. These conditions can be beneficial to higher order modes. In this case, the present study can be seen as first order approximation.

Acknowledgment

This work, within the SINAPS@ project, benefited from French state funding managed by the National Research Agency under program RNSR Future Investments bearing reference No. ANR-11-RSNR-0022-04. The research reported in this paper has been supported in part by the SEISM Paris Saclay Research Institute.

References

[1] J.W Wallace. Modelling issues for tall reinforced concrete core wall buildings. *The structural design of tall and special buildings*, 16(5):615–632, 2007.

[2] C. Balkaya and E. Kalkan. Performance based seismic evaluation of shear-wall dominant building structures. In *Fifth International Congress on Advances in Civil Engineering*, pages 1–23. Istanbul Technical University, September 2002.

[3] A. Habasaki and et al. Multi-directional loading test for rc seismic shear walls. In *Proceedings of 12th World Conference on Earthquake Engineering*, pages 454–462. New Zealand Society for Earthquake Engineering, January 2000.

[4] J. Gerber and G. van Zijl. Alternative wall-to-slab connection systems in reinforced concrete structures. *Journal of the South African Institution of Civil Engineering*, 59(3):36–47, 2017.

[5] M. Memon. *Strength and stiffness of shear wall-floor slab connections*. PhD thesis, University of Glasgow, 1984.

[6] S. Pantazopoulou and I. Imran. Slab-wall connections under lateral forces. *ACI Structural Journal*, 89(5):515–527, 1992.

[7] N. Ile and J. Reynouard. Seismic behaviour of r/c shear wall structures designed according to the french ps92 and ec8 codes: a comparison between shaking-table response data and 2d modelling. In *Proceedings of 12th World Conference on Earthquake Engineering*, pages 1752–1760. New Zealand Society for Earthquake Engineering, January 2000.

[8] A. Kudzys and A. Kudzys. Evaluation of wall-slab connection behaviour under extreme lateral actions. *Statyba*, 2(8):35–44, 1996.

[9] A. Kudzys and A. Kudzys. Strength and safety of slab-wall joints of reinforced concrete buildings under gravity and lateral loads. *Statyba*, 2(8):45–51, 1996.

[10] A. Al-Aghbari, N. Rahman, and S. Hamzah. Structural performance of two types of wall slab connection under out-of-plane lateral cyclic loading. *Journal of Engineering science and technology*, 7(2):177–194, 2012.

[11] S. Chun and T. Ha. Cyclic behavior of wall-slab joints with lap splices of cold-straightened rebars and mechanical splices. *Journal of Structural Engineering*, 141(2):1441–1446, 2014.

[12] S. Kaushik and K. Dasgupta. Seismic damage in shear wall-slab junction in rc buildings. *Procedia Engineering*, 144:1332–1339, 2016.

[13] G. Cocchi. Elastic-static analysis of shear wall/slab-frame systems using the framework method. *Computers & structures*, 54(2):303–313, 1995.

[14] S. Greeshma, C. Rajesh, and K. Jaya. Seismic behaviour of shear wall–slab joint under lateral cyclic loading. *Asian Journal of Civil Engineering (Building and Housing)*, 13:455–464, 2012.

[15] R. Surumi, K. Jaya, and S. Greeshma. Modelling and assessment of shear wall–flat slab joint region in tall structures. *Arabian Journal for Science and Engineering*, 40(8):2201–2217, 2015.

[16] S. Kaushik and K. Dasgupta. Seismic behaviour of rc slab–shear wall assemblage using non-linear static and dynamic analyses. In *Structural Engineering Convention (SEC-2016)*, pages 1234–1239. CSIR-SERC, 2016.

[17] R. Surumi, S. Greeshma, and K. Jaya. Reinforced concrete structural wall-floor slab connection - state of the art. In *ISET GOLDEN JUBILEE SYMPOSIUM*, pages 1–13. Indian Society of Earthquake Technology, October 2012.

[18] B. Chiaia, E. Barchiesi, V. De Biagi, and L. Placidi. A novel worst-case-based structural resilience index: Definition, computation and applications to portal frame structures. *Mechanics Research Communications*, 2019.

[19] J. Mottershead, M. Link, and M. Friswell. The sensitivity method in finite element model updating: a tutorial. *Mechanical systems and signal processing*, 25(7):2275–2296, 2011.

[20] J. Mottershead and M. Friswell. Model updating in structural dynamics: a survey. *Journal of sound and vibration*, 167(2):347–375, 1993.

[21] M. Friswell and J. Mottershead. *Finite element model updating in structural dynamics*. Springer Science & Business Media, 1995.

[22] L. Humbert. *Recalage des modèles éléments finis à partir de mesures vibratoires*. PhD thesis, Ecole centrale de Lyon, 1999.

[23] E. Markiewicz, B. Langrand, and D. Notta-Cuvier. A review of characterisation and parameters identification of materials constitutive and damage models: from normalised direct

approach to most advanced inverse problem resolution. *International Journal of Impact Engineering*, 110:371–381, 2017.

[24] J. Zapico-Valle, R. Alonso-Camblor, M. González-Martínez, and M. García-Diéguez. A new method for finite element model updating in structural dynamics. *Mechanical Systems and Signal Processing*, 24(7):2137–2159, 2010.

[25] Q. Jiang, Y. Sun, B. Yi, T. Li, and F. Xiong. Inverse analysis for geomaterial parameter identification using pareto multiobjective optimization. *International Journal for Numerical and Analytical Methods in Geomechanics*, 42(14):1698–1718, 2018.

[26] L. Nguyen-Tuan, C. Könke, V. Bettzieche, and T. Lahmer. Damage identification using inverse analysis in coupled thermo-hydro-mechanical problems applied to masonry dams. *International Journal for Numerical and Analytical Methods in Geomechanics*, 42(2):256–273, 2018.

[27] A. Murakami, H. Shinmura, S. Ohno, and K. Fujisawa. Model identification and parameter estimation of elastoplastic constitutive model by data assimilation using the particle filter. *International Journal for Numerical and Analytical Methods in Geomechanics*, 42(1):110–131, 2018.

[28] S. Levasseur, Y. Malécot, M. Boulon, and E. Flavigny. Soil parameter identification using a genetic algorithm. *International Journal for Numerical and Analytical Methods in Geomechanics*, 32(2):189–213, 2008.

[29] K. Hossain. Non-linear performance of slabs in coupled shear wall structures. *Advances in Structural Engineering*, 6(4):339–352, 2003.

[30] A. Daryan and et al. Behavior of semi-rigid connections and semi-rigid frames. *The Structural Design of Tall and Special Buildings*, 23(3):210–238, 2014.

[31] P. Ladevèze and D. Leguillon. Error estimate procedure in the finite element method and applications. *SIAM Journal on Numerical Analysis*, 20(3):485–509, 1983.

[32] P. Ladevèze, D. Nedjar, and M. Reynier. Updating of finite element models using vibration tests. *AIAA journal*, 32(7):1485–1491, 1994.

[33] A. Chouaki. *Recalage de modèles dynamiques de structures avec amortissement.* PhD thesis, Cachan, Ecole normale supérieure, 1997.

[34] V. Decouvreur, P. Ladevèze, and P. Bouillard. Updating 3d acoustic models with the constitutive relation error method: A two-stage approach for absorbing material characterization. *Journal of sound and vibration*, 310(4-5):985–997, 2008.

[35] P. Charbonnel, P. Ladevèze, F. Louf, and C. Le Noac'h. A robust cre-based approach for model updating using in situ measurements. *Computers & Structures*, 129:63–73, 2013.

[36] A. François and T. Philippe. *Structural Elements*. Butterworth-Heinemann, 2005.

[37] Cast3m. *CEA, Logiciel de calcul par éléments finis en mécanique des structures et des fluides, available at http://www-cast3m.cea.fr/index.php*, 2018.

[38] E. Herve-Secourgeon, F. Gatuingt, A. Guilloux, C. Oliver-Leblond, and F. Voldoire. Toward a model for wall-slab junctions in nuclear reinforced concrete structures: first steps. In *Proceedings of International Conference on Technological Innovations in Nuclear Civil Engineering - TINCE 2018*. Paris-Saclay, France, August 2018.

[39] H. Sun and O. Büyüköztürk. Probabilistic updating of building models using incomplete modal data. *Mechanical Systems and Signal Processing*, 75:27–40, 2016.

[40] Z. Mróz and T. Lekszycki. Optimal support reaction in elastic frame structures. *Computers & Structures*, 14(3-4):179–185, 1981.

Resistance class		$C30/37$
Feature Compression Know	f_{ck}	$30MPa$
Concrete Tensile Strength	f_{ctm}	$2.9MPa$
Concrete Young modulus	E_{cm}	$32000MPa$
Concrete Poisson ratio	ν_c	0.2
Concrete Unity weight	ρ_c	$2500kg/m^3$
Additional mass per slab		$938kg$
Steel Young modulus	E_s	$200GPa$
Steel Poisson ratio	ν_s	0.3
Steel Unity weight	ρ_s	$7850kg/m^3$

Table 1: Mock-up material properties

Mock-up response	Mode 1 (Hz)	Mode 2 (Hz)	Mode 3 (Hz)
Experimental results	8.32	10.0	14.57
Before identification	4.33	6.92	23.90
After identification considering all sensors	7.92	9.16	15.09
After identification with selected sensors	8.34	9.52	15.12

Table 2: Mock-up frequencies comparison

Mock-up response	Mode 1 Error(%)	Mode 2 Error(%)	Mode 3 Error(%)
Before identification	-48.1	-30.8	64.0
After identification considering all sensors	-4.8	8.4	3.57
After identification with selected sensors	0.24	-4.80	3.77

Table 3: Mock-up frequencies error comparison

List of Figures

Figure 24: Third mode. Comparison between numerical (left side) and experimental (right side)

Figure 25: Evolution of the MAC measure. (a) MAC axis (b) Experiments versus Numerical Model before updating (c) Experiments versus Numerical Model updated considering all sensors (d) Experiments versus Numerical Model after sensors selection

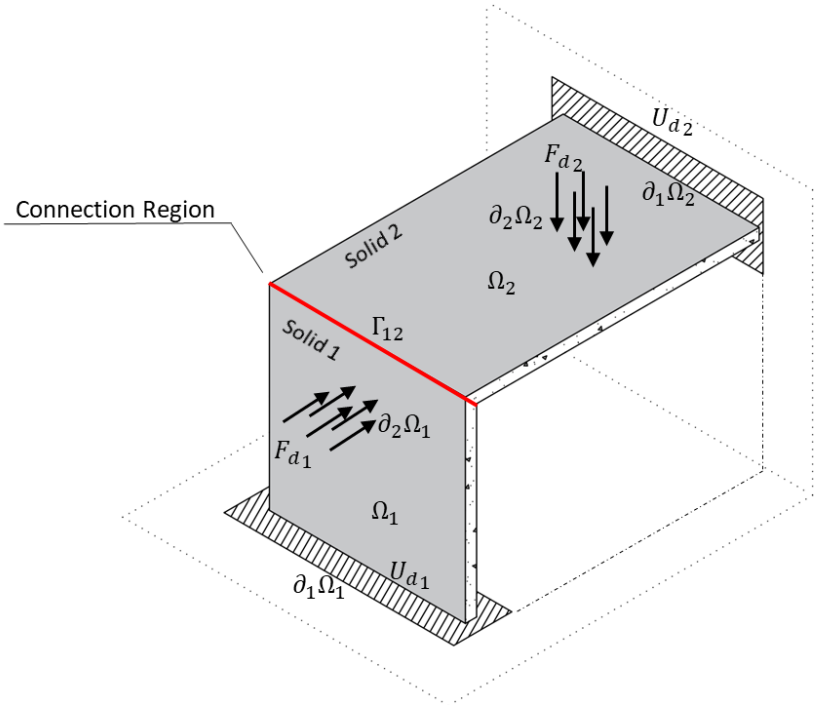

Figure 1: Reference configuration

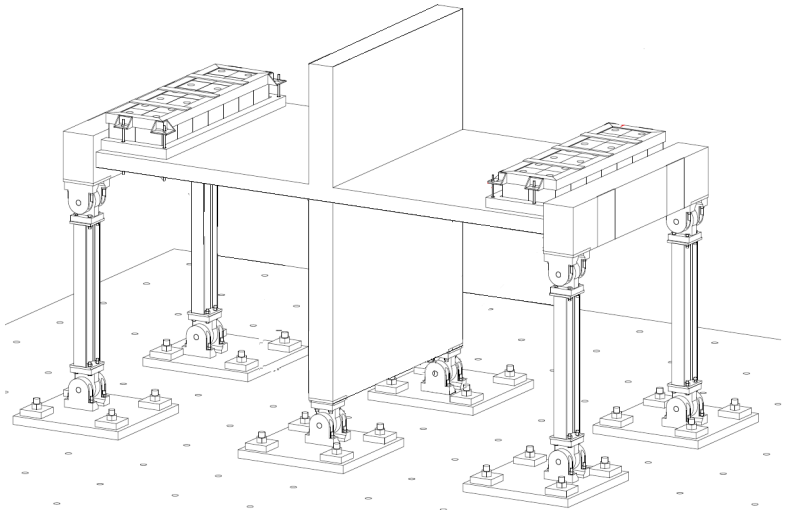

Figure 2: Experimental 1:4 reduced scale structure (mock-up)

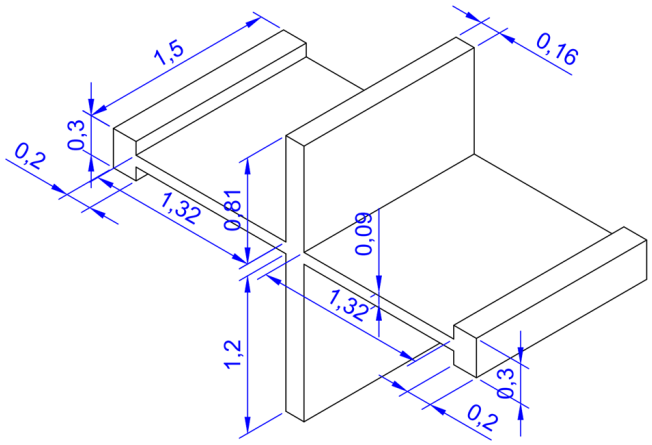

Figure 3: Mock-up geometry (dimensions in meters)

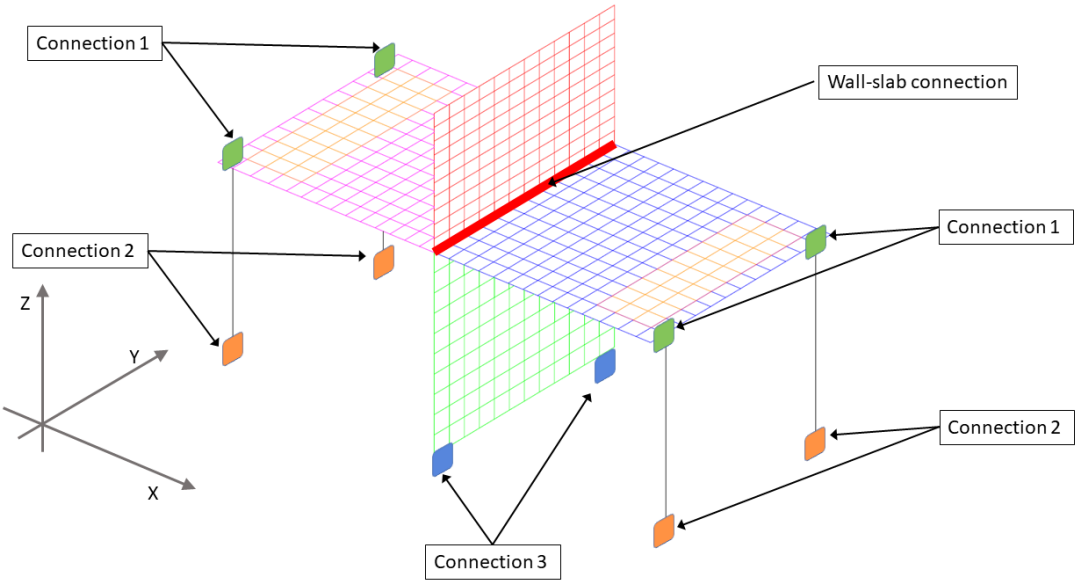

Figure 4: Numerical model with the corresponding connection type depending on its position

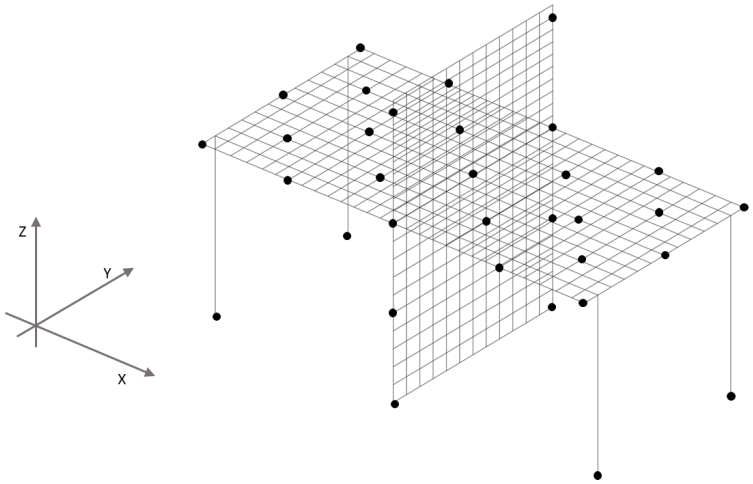

Figure 5: Correspondent triaxial sensor positions on the numerical model

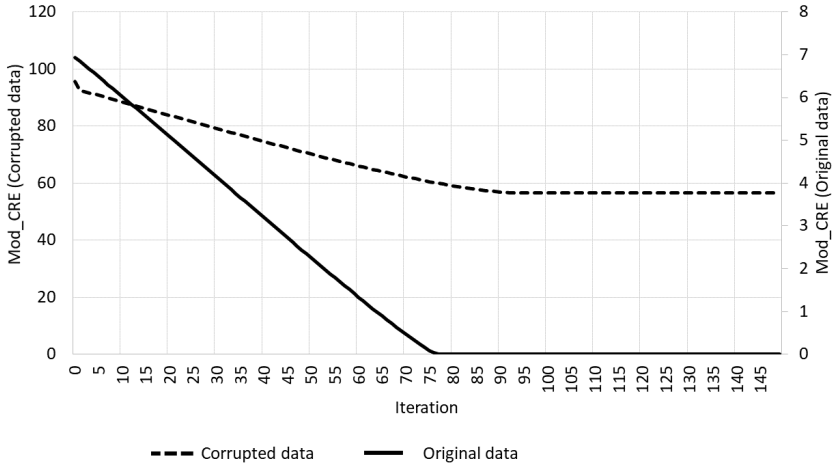

Figure 6: Comparison between the convergence history for the different types of reference data

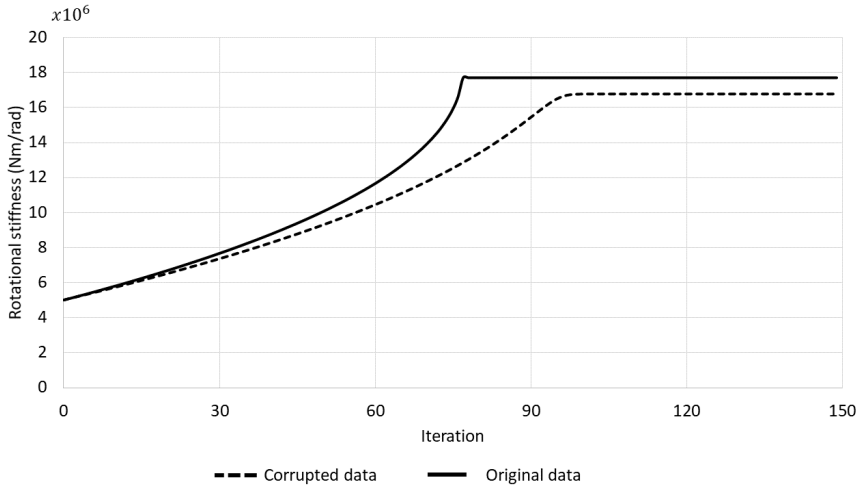

Figure 7: Convergence of the rotational stiffness for the different types of reference data

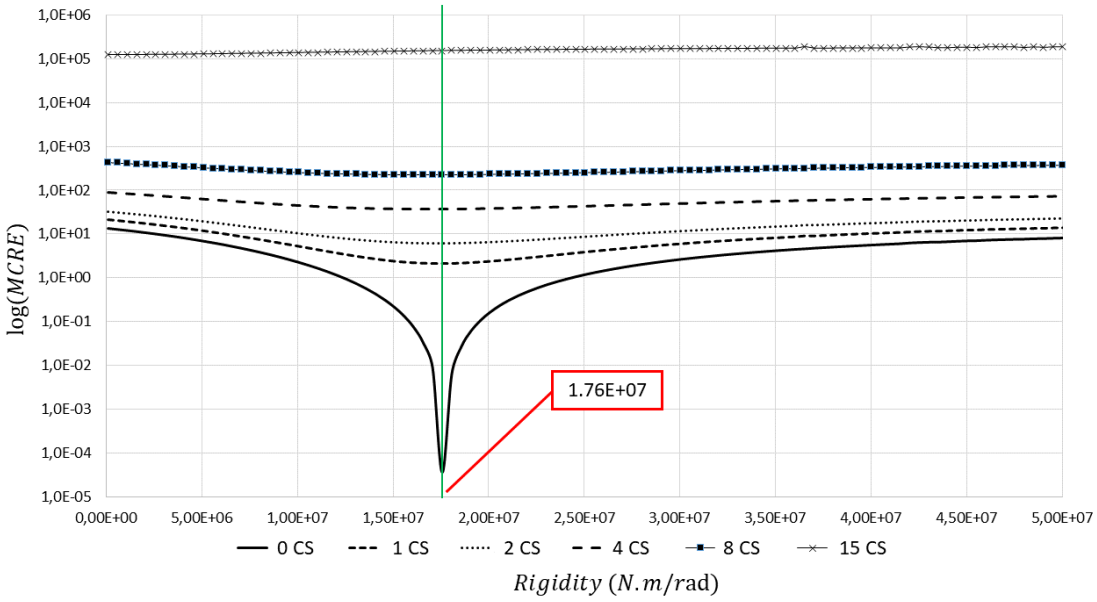

Figure 8: Evolution of MCRE according to the increase in the number of corrupt sensors

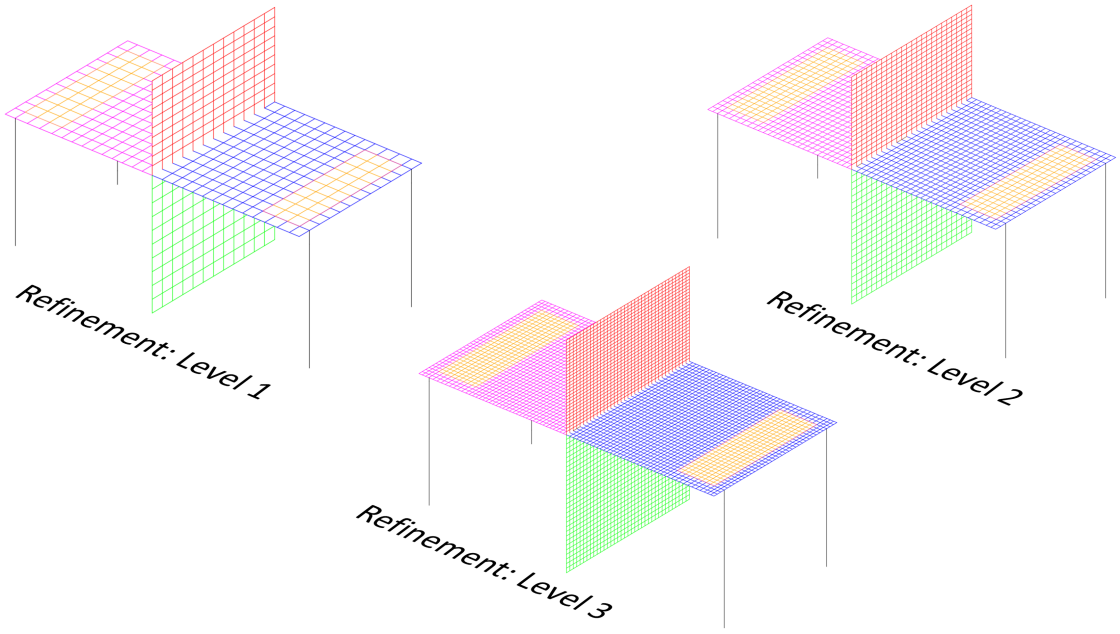

Figure 9: Refinement level. Level 1: 616 elements. Level 2: 2344 elements. Level 3: 5224 elements

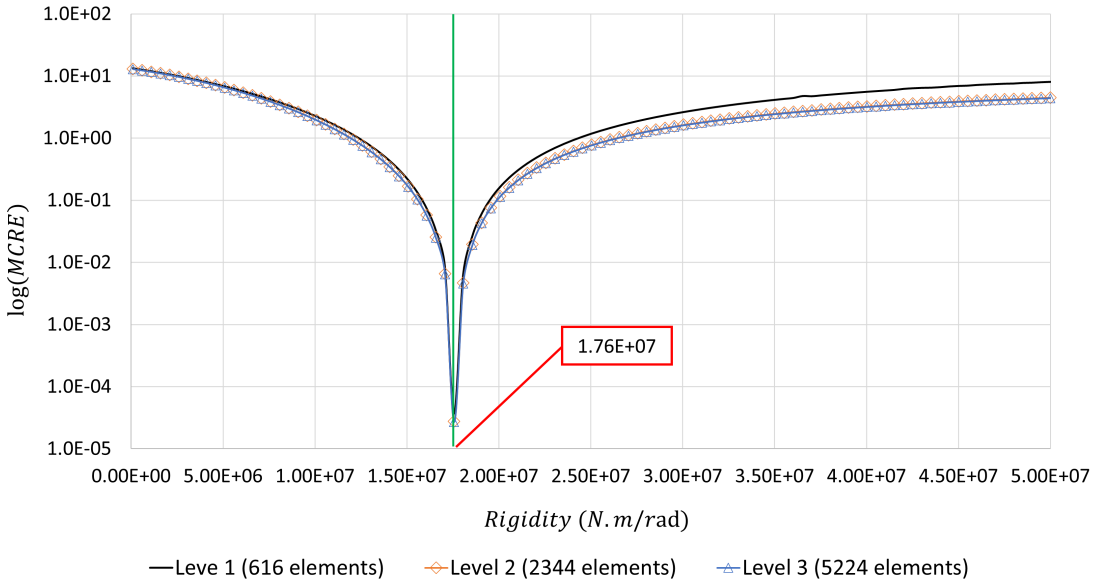

Figure 10: Influence of the mesh refinement on the identification process

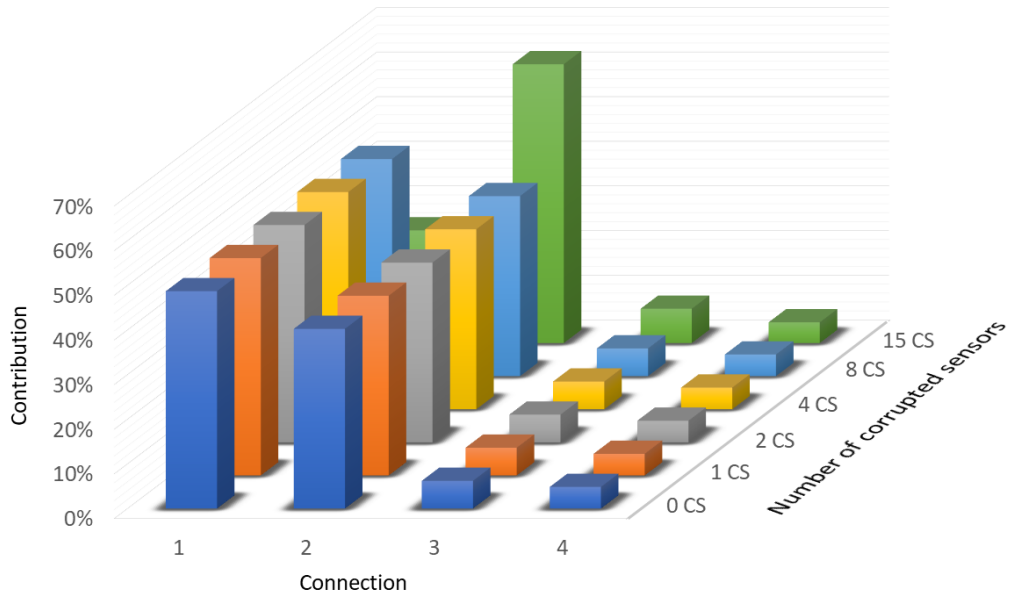

Figure 11: CRE correction indicator varying with the number of corrupted sensors

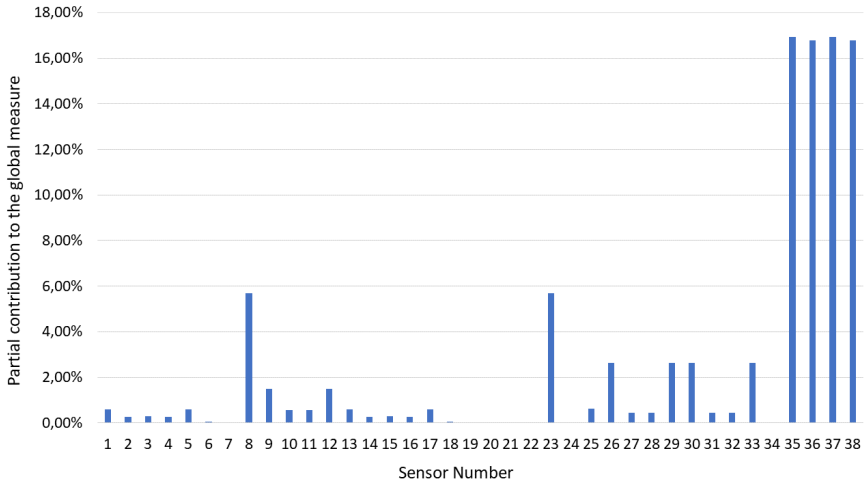

Figure 12: Partial Contribution to the error measure without corrupt sensors (0 CS)

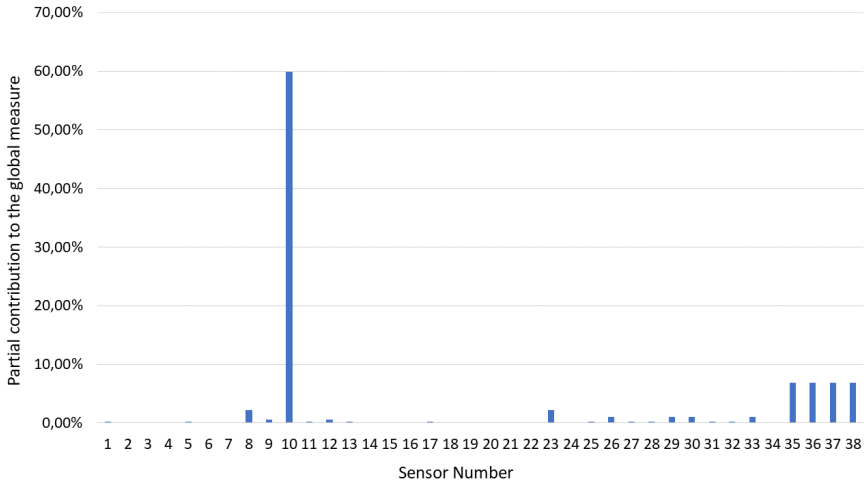

Figure 13: Partial Contribution to the error measure with one corrupt sensor (1 CS)

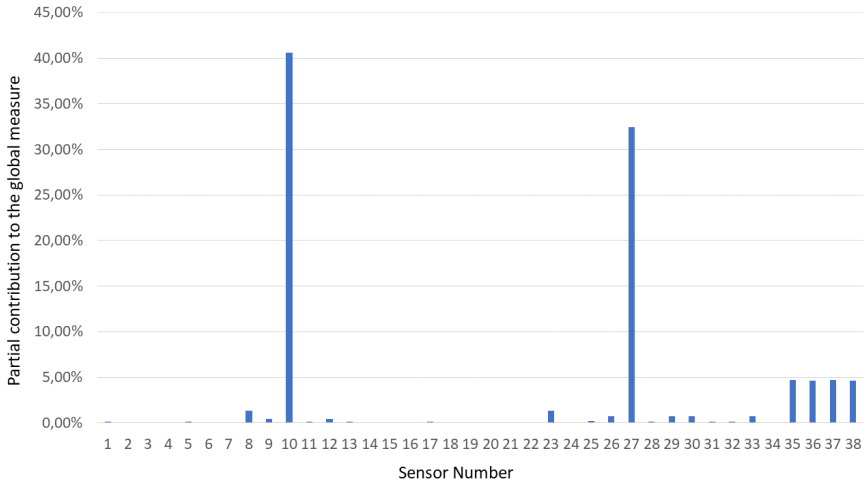

Figure 14: Partial Contribution to the error measure with two corrupt sensors (2CS)

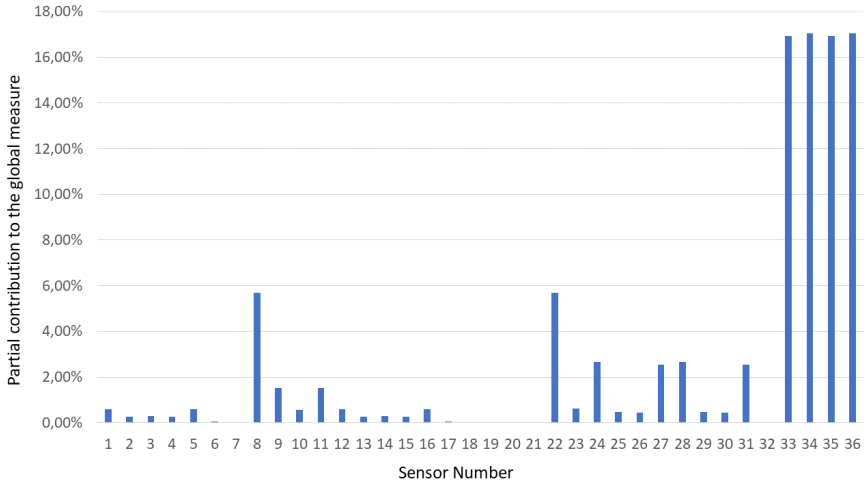

Figure 15: Partial Contribution to the error measure removing the defective sensors

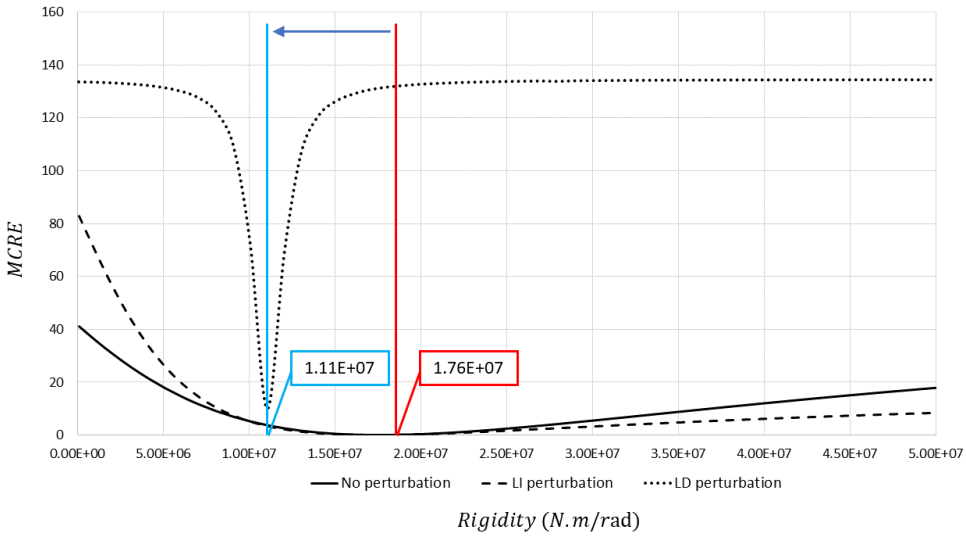

Figure 16: Influence of boundary conditions perturbation: identification of the rotational rigidity along y axis at connection 3 for a perturbation at connection 2

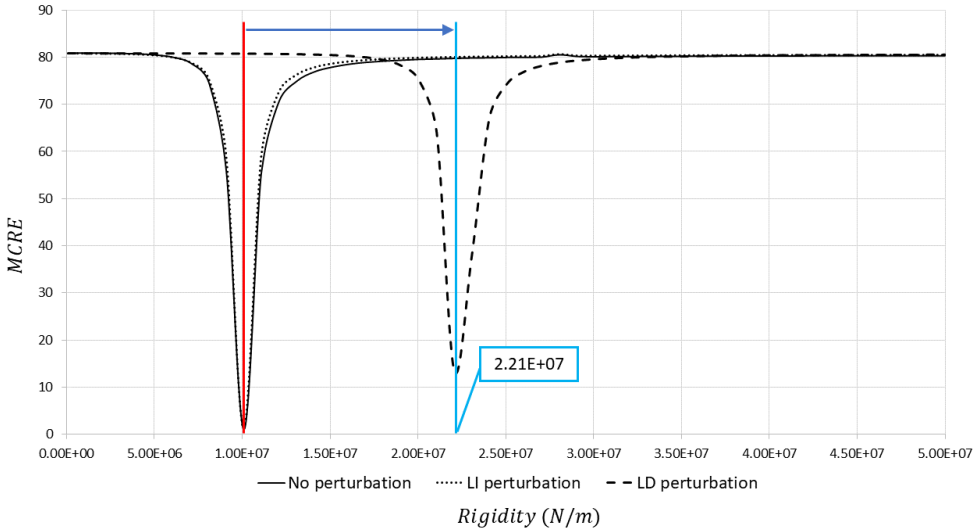

Figure 17: Influence of boundary conditions perturbation: identification of the translational rigidity along y axis at connections type 2 for a perturbation at connection 1

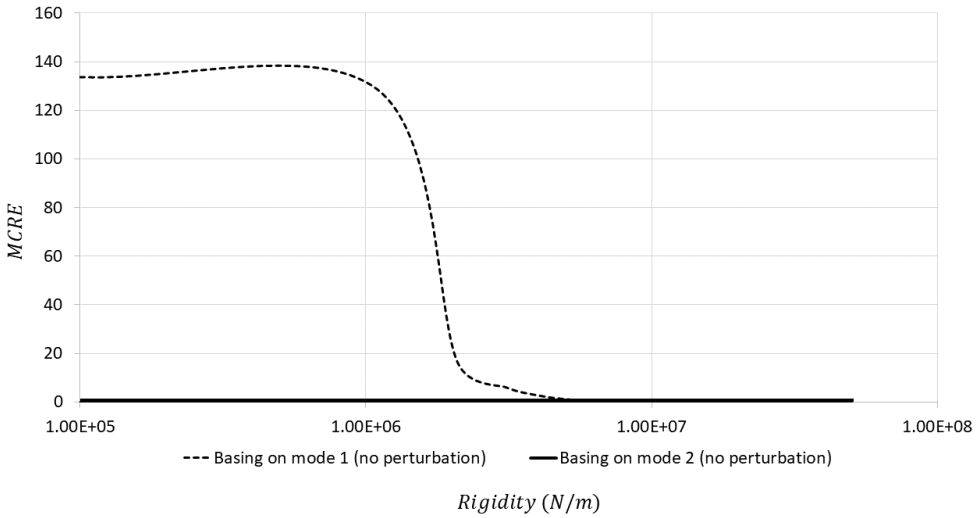

Figure 18: Identification of translational parameter along z direction at the wall/slab connection considering the first and second modal shapes

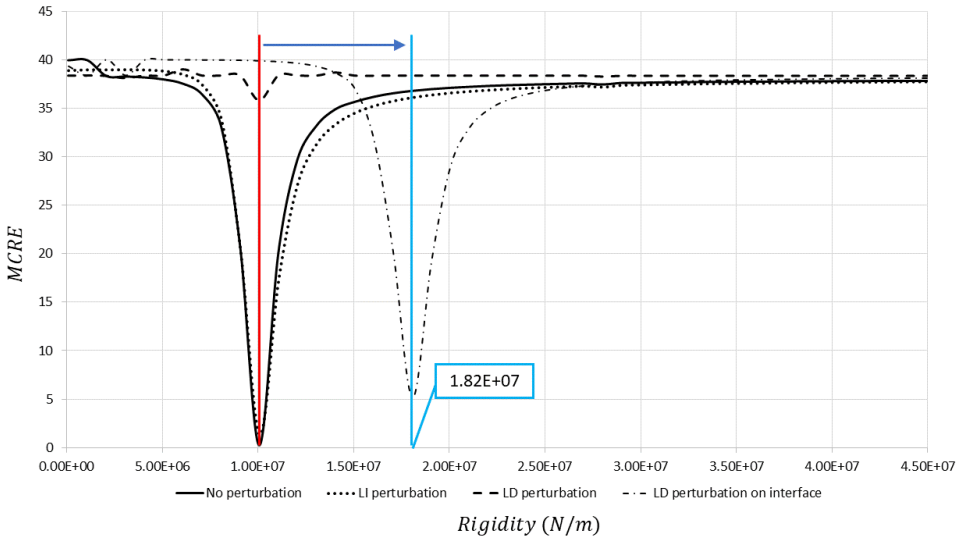

Figure 19: Influence of the boundary conditions and interface parameter on the identification process for the translational rigidity along the z direction at the wall/slab connection considering the third mode shape

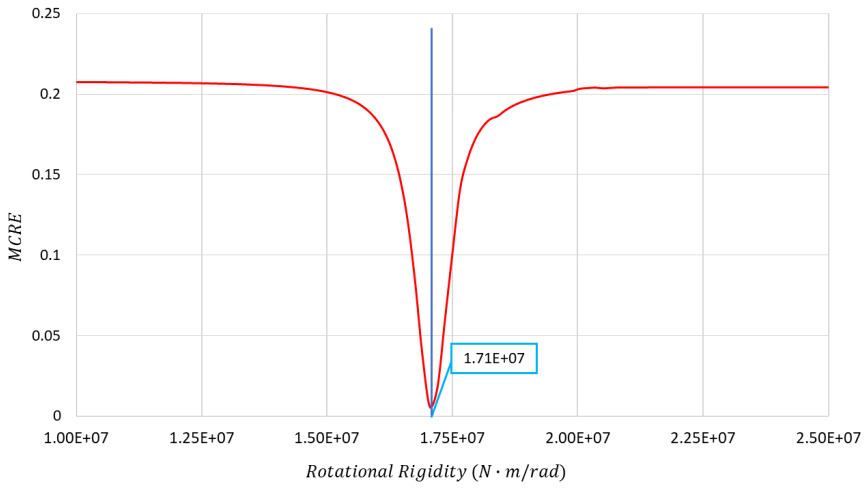

Figure 20: Rotational stiffness identification

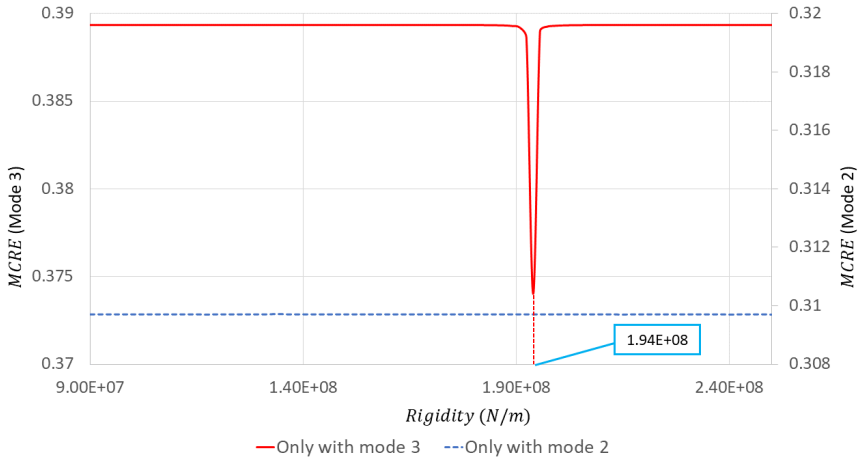

Figure 21: Translational stiffness identification considering the second and third modes

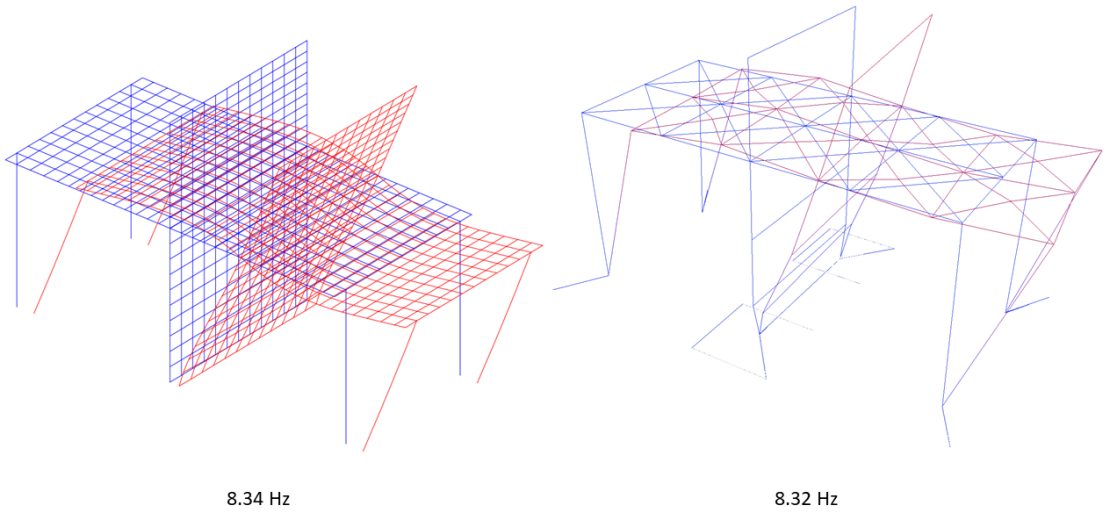

Figure 22: First mode. Comparison between numerical (left side) and experimental (right side)

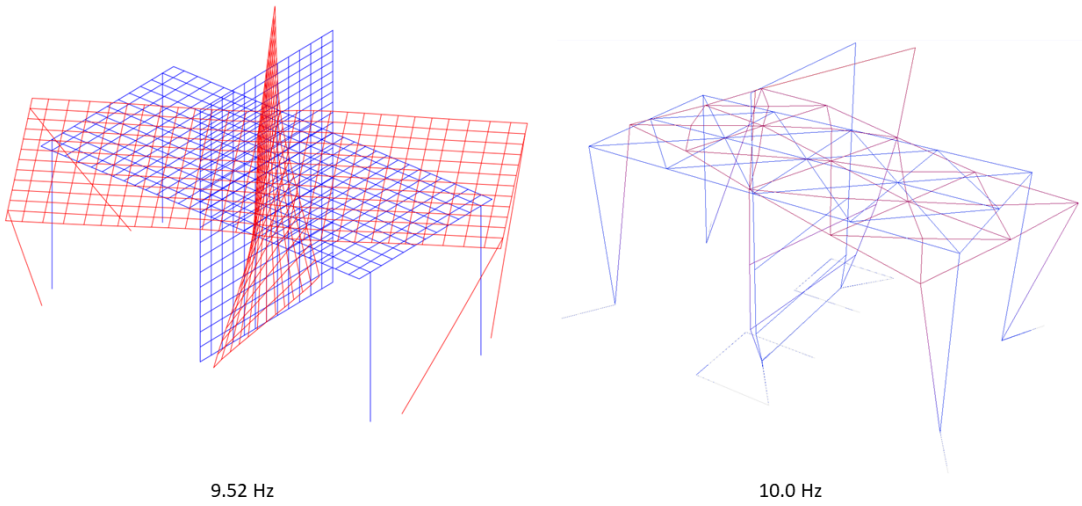

Figure 23: Second mode. Comparison between numerical (left side) and experimental (right side)

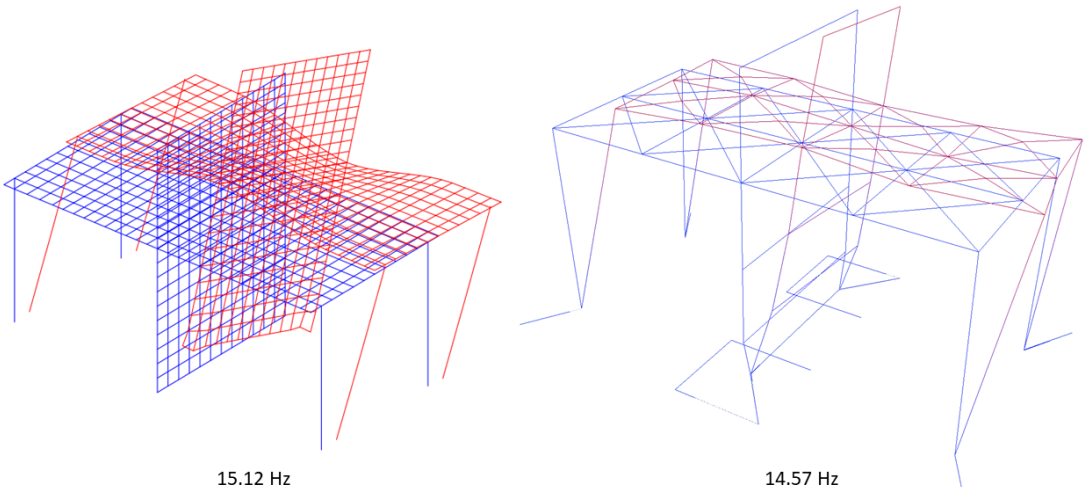

Figure 24: Third mode. Comparison between numerical (left side) and experimental (right side)

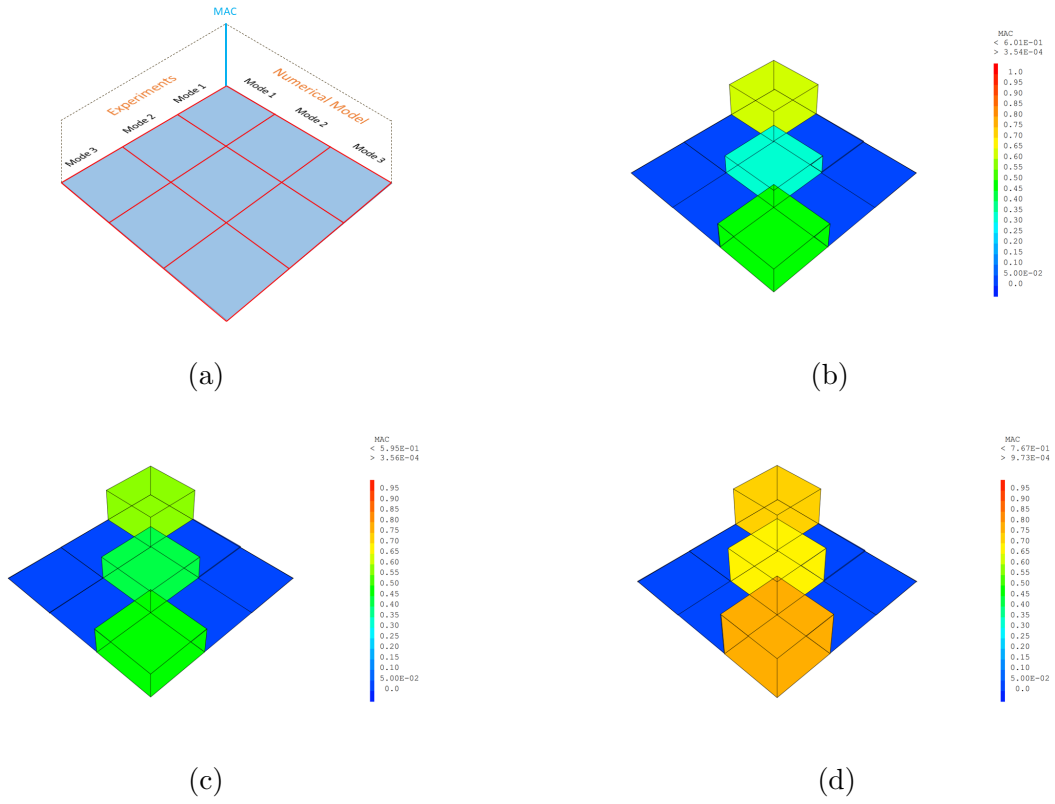

Figure 25: Evolution of the MAC measure. (a) MAC axis (b) Experiments versus Numerical Model before updating (c) Experiments versus Numerical Model updated considering all sensors (d) Experiments versus Numerical Model after sensors selection